Title: Climate explains geographic and temporal variation in mosquito-borne disease dynamics on two continents

Jamie M. Caldwell[1], A. Desiree LaBeaud[2], Eric F. Lambin[3,4], Anna M. Stewart-Ibarra[5,6], Bryson A. Ndenga[7], Francis M. Mutuku[8], Amy R. Krystosik[2], Efraín Beltrán Ayala[9], Assaf Anyamba[10], Mercy J. Borbor-Cordova[11], Richard Damoah[12], Elysse N. Grossi-Soyster[2], Froilán Heras Heras[13], Harun N. Ngugi[14,15], Sadie J. Ryan[16-18], Melisa M. Shah[19], Rachel Sippy[13,20,21], Erin A. Mordecai[1]

[1] Department of Biology, Stanford University, 371 Serra Mall, Stanford, California, USA

[2] Department of Pediatrics, Division of Infectious Diseases, Stanford University, 300 Pasteur Drive, Stanford, California, USA

[3] School of Earth, Energy & Environmental Sciences, and Woods Institute for the Environment, Stanford University, Stanford, California 94305, USA.

[4] Georges Lemaître Earth and Climate Research Centre, Earth and Life Institute, Université catholique de Louvain, 1348 Louvain-la-Neuve, Belgium.

[5] Department of Medicine and Department of Public Health and Preventative Medicine, SUNY Upstate Medical University, Syracuse, NY, USA

[6] InterAmerican Institute for Global Change Research (IAI), Montevideo, Uruguay

[7] Centre for Global Health Research, Kenya Medical Research Institute, Kisumu, Kenya

[8] Department of environment and health sciences, technical university of Mombasa, Mombasa, Kenya

[9] Technical University of Machala, Machala, Ecuador

[10] Universities Space Research Association and NASA Goddard Space Flight Center, Greenbelt, MD, USA.

[11] Facultad de Ingeniería Marítima y Ciencias del Mar, Escuela Superior Politécnica del Litoral, ESPOL, Guayaquil, Ecuador

[12] Morgan State University and NASA Goddard Space Flight Center, Greenbelt, MD, USA.

[13] Center for Research SUNY-Upstate-Teófilo Dávila Hospital, Machala, Ecuador

[14] Department of Biological Sciences, Chuka University, Chuka, Kenya

[15] Department of Zoology, School of Biological Sciences University of Nairobi, Nairobi, Kenya

[16] Emerging Pathogens Institute, University of Florida, Gainesville, Florida

[17] Quantitative Disease Ecology and Conservation (QDEC) Lab, Department of Geography, University of Florida, Gainesville, Florida;

[18] School of Life Sciences, University of KwaZulu, Natal, South Africa

[19] Department of Medicine, Division of Infectious Diseases, Stanford University, 300 Pasteur Drive, Stanford, California, USA

[20] Institute for Global Health and Translational Science, SUNY-Upstate Medical University, Syracuse, NY, USA

[21] Department of Medical Geography, University of Florida, Gainesville, FL, USA

Abstract:

Climate drives population dynamics, but when the underlying mechanisms are unresolved, studies can lead to seemingly context-dependent effects of climate on natural populations. Climate-sensitive vector-borne diseases such as dengue, chikungunya, and Zika are one example where climate appears to have opposing effects in different contexts. In this study, our objective was to test the extent to which a mathematical model, parameterized with climate-driven mosquito physiology measured in laboratory studies, predicts observed vector and disease dynamics in the field across ecologically and culturally distinct settings in Ecuador and Kenya. The model incorporates different rain functions and time lags. We show that the climate-driven model generates a range of disease dynamics consistent with observations of *Aedes aegypti* abundances and laboratory-confirmed arboviral incidence with varying levels of accuracy (28 – 85% for vector dynamics, 36 – 88% for human disease dynamics). Further, we find that the model predicted vector dynamics better in sites with a smaller proportion of young children in the population, lower mean temperature, and a larger proportion of homes without window screens and made of cement; the model predicted human disease dynamics better in sites with lower annual rainfall and a larger proportion of homes that spray insecticide. A mechanistic model that robustly captures the influence of climate on viruses transmitted by *Aedes aegypti* provides critical information to help guide future intervention efforts and improve climate change predictions.

Introduction:

Climate is a major driver of species interactions and population dynamics, but the mechanisms underlying the ecological effects of climate are often poorly understood and rarely tested in the field [1]. One of the primary ways that climate impacts populations is through its effects on species' vital rates [2]. However, these mechanistic effects may appear context dependent in the field because multiple climate variables can act synergistically, with each climate variable potentially affecting multiple vital rates, and their impacts may be nonlinear, changing direction and relative importance across a gradient of conditions [3,4]. Therefore, paradoxically, while climate is thought to be one of the most pervasive drivers of ecological processes, its directional and dynamical effects on systems are often poorly understood and difficult to predict. Vector-borne diseases provide an interesting case study to test whether climate sensitive traits measured in controlled, laboratory settings can reproduce the wide range of dynamics observed in the field. For example, transmission of mosquito-borne viral (arboviral) diseases such as dengue, chikungunya, and Zika occur along a spectrum from low levels of year-round endemic transmission [5] to large seasonal or interannual outbreaks [6]. We hypothesize that important features of these differing dynamics arise due to regional differences in climate, where the magnitude and direction of the effects of climate on vector and disease dynamics differ [7–12] because of the subset of climate conditions that occur in a given location or season.

Understanding the mechanisms that drive disease dynamics can help address two critically important research priorities for arboviruses like dengue, chikungunya, and

Zika: assessing intervention strategies and projecting climate change impacts on disease dynamics. While phenomenological models often replicate arboviral disease dynamics remarkably well [13], mechanistic models that capture mosquito population dynamics and interactions between mosquitoes and humans will provide more realistic predictions for the effects of different interventions or projected changes in climate. With no widely available vaccine, vector control (e.g., larvicides, *Wolbachia*-infected mosquito releases) remains the primary method for preventing arboviral disease transmission, and, like other vector-borne diseases with complex transmission dynamics, model simulations can help guide effective intervention efforts [14,15]. Further, mechanistic models are better suited to predict how climate change will impact future disease burden and distribution, as projected climate conditions are outside the current arboviral climate niche space [16].

Dengue, chikungunya, and Zika are climate-sensitive diseases because of the ecology of *Aedes aegypti*, the primary disease vector. *Ae. aegypti* are anthropophilic, globally distributed mosquitoes that breed in artificial containers with standing water [17,18]. All mosquito and parasite traits that are important for transmission and linked to metabolism, such as reproduction, development, survival, biting rate, and extrinsic incubation period, are temperature dependent with an intermediate thermal optimum [19–21]. Humidity is positively associated with mosquito survival because the high surface area to volume ratio of mosquitoes exposes them to desiccation [22,23]. Standing water from rainfall provides essential larval and pupal habitat for mosquitoes, but the relationship is complex because heavy rainfall can flush away breeding habitats [24–26] and water storage

practices during drought can increase water availability, mosquito abundance, and contact between mosquitoes and people [27–29].

In this study, our goal was to test the extent to which climate-driven mosquito traits drive disease dynamics across two geographically distinct regions and to characterize additional climatological, ecological, and social factors that may mediate the effects of climate on disease dynamics. We built on previous mechanistic and semi-mechanistic models [30–35] by combining a suite of temperature, humidity, and rainfall dependent trait functions into one epidemiological model. We validated the model with *Ae. aegypti* abundances and laboratory-confirmed dengue, chikungunya, and Zika cases from two equatorial countries with distinct socioeconomic, geographic, cultural, and disease transmission settings: Ecuador and Kenya (Fig. 1, Table 1). The study sites within each country were distributed across a gradient of temperature, humidity, and rainfall. Previous studies have found that *Ae. aegypti* and dengue were positively associated with warm and wet conditions in Ecuador and Kenya [6,36–38], although other *Ae. aegpyti*-vectored arboviruses in Kenya such as chikungunya have been associated with warm and dry conditions [39]. Both countries have hyperendemic transmission of all four dengue serotypes and have recently experienced outbreaks of chikungunya; yet, arboviral transmission dynamics differ in each country. In Ecuador, dengue is a re-emerging disease with large seasonal epidemics that frequently result in severe dengue [6]; by contrast, in Kenya, dengue is transmitted at low levels year-round [5] and intermittent self-limiting outbreaks often go undetected [40]. Further, compared with South America, severe dengue is rare in sub-Saharan Africa, perhaps because African strains of *Ae.*

aegpyti have lower susceptibility to all four dengue serotypes [41], and/or because people of African ancestry are less susceptible to severe dengue [42].

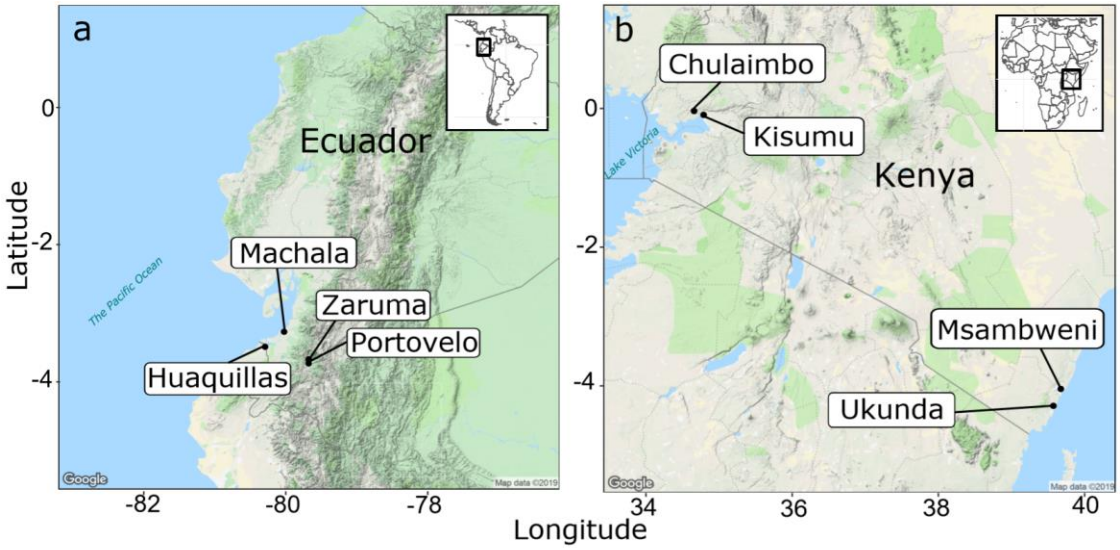

Figure 1: Study sites within two equatorial countries: (a) Ecuador in South America and (b) Kenya in East Africa.

Table 1: Study sites differ geographically, climatologically, and socioeconomically. [1]Urbanization is measured as nighttime light from the built environment from NASA's Black Marble product suite [43]. [2]Mean annual normalized difference vegetation index (NDVI) is a proxy for photosynthesis and measured as a difference in spectral reflectance in the visible and near-infrared regions from NASA/NOAA MODIS (MOD13A1) [44]. [3]Dominant land cover type is measured and classified from spectral and temporal features from NASA/NOAA MODIS (MCD12Q1) [45]. Land cover types include (9) Tree cover 10 - 30%, (10) Dominated by herbaceous annuals, (13) >30% impervious surface area, and (14) 40 - 60% mosaics of small-scale cultivation.

	Huaquillas, Ecuador	Machala, Ecuador	Portovelo, Ecuador	Zaruma, Ecuador	Chulaimbo, Kenya	Kisumu, Kenya	Msmabweni, Kenya	Ukunda, Kenya
Site characteristics								
Elevation (m)	15	6	645	1,155	1,328	1,100	4	8
Location	Coastal	Coastal	Inland	Inland	Inland	Inland	Coastal	Coastal
Urbanization ($nW*cm^2*sr^{-1}$)[1]	255	255	233	116	14	255	255	171
Mean annual NDVI[2]	0.22	0.12	0.61	0.57	0.63	0.35	0.33	0.52
Dominant land cover type[3]	13	13	9	10	14	13	13	10
Climate								
Mean temperature (°C)	26	26	25	22	24	26	28	28
Mean relative humidity (%)	81	84	81	86	69	50	76	78
Mean annual rainfall (mm)	317	669	500	1115	1125	810	1048	922
Demographics								
Human population size	57,366	279,887	13,673	25,615	7,304	491,893	15,371	80,193
Population <5 years (%)	10	9	9	8	12	12	13	14
Population of African ancestry (%)	5.1	6.0	3.3	2.9	100.0	100.0	100.0	100.0
Housing quality (% houses)								
Piped water inside home	90	91	100	96	2	4	3	11
No screens on windows	7	60	91	99	74	78	43	21
House materials (cement/mud/wood)	87/5/0	87/8/5	95/0/5	93/1/1	29/70/0	77/17/0	38/62/0	51/47/0
Exposure, vulnerability, and adaptive capacity								
Arboviruses present	dengue, chikungunya, Zika				>200 documented including dengue, chikungunya, Yellow fever, Rift Valley fever, West Nile fever, O'nyong-nyong			
Insecticide use (% houses)	19	28	46	37	0	0	11	55
Bednet use (% houses)	77	55	15	21	93	92	0	96
Other vector control strategies used	Ultra-low volume fumigation with malathion (organophosphate) and community mobilization to eliminate larval habitats				Mosquito coils			
Annual gross domestic product by country (2018)	$177 billion USD				$85.98 billion USD			

Results:

Relationship between model predictions and observed disease dynamics

The dynamic susceptible, exposed, infectious – susceptible, exposed, infectious, removed (SEI-SEIR) compartmental model parameterized with temperature-, humidity-, and

rainfall-dependent mosquito life history traits (Fig. 2) generated mosquito and disease dynamics reflective of observed dynamics across sites and through time with varying levels of accuracy (Fig. 3, Table 2). Model-predicted mosquito abundances were significantly correlated with field-collected observations of mosquito abundances in seven of the eight study sites, explaining 28 – 85% of site-level variation through time based on pairwise correlations with an adjusted p-value (following [46]). Based on surveys conducted across all vector life stages in Kenya (only adult mosquitoes were collected in the Ecuador surveys), the SEI-SEIR model explained variation in the abundance of adult mosquitoes (28 – 45%) better than pupae (23 – 33%), late instars (21 – 34%), early instars (20 – 36%), and eggs (33 – 42%), likely because the model did not explicitly incorporate other mosquito life history stages. Model-predicted disease cases were significantly correlated with laboratory-confirmed arboviral incidence in seven of the eight study sites, explaining 36 – 88% of site-level variation through time (within sites with statistically significant pairwise correlations). Overall, the model reproduced mosquito and arboviral dynamics much better than random (i.e., 0% correlation) and in general, predicted disease dynamics slightly better for sites in Ecuador compared with Kenya.

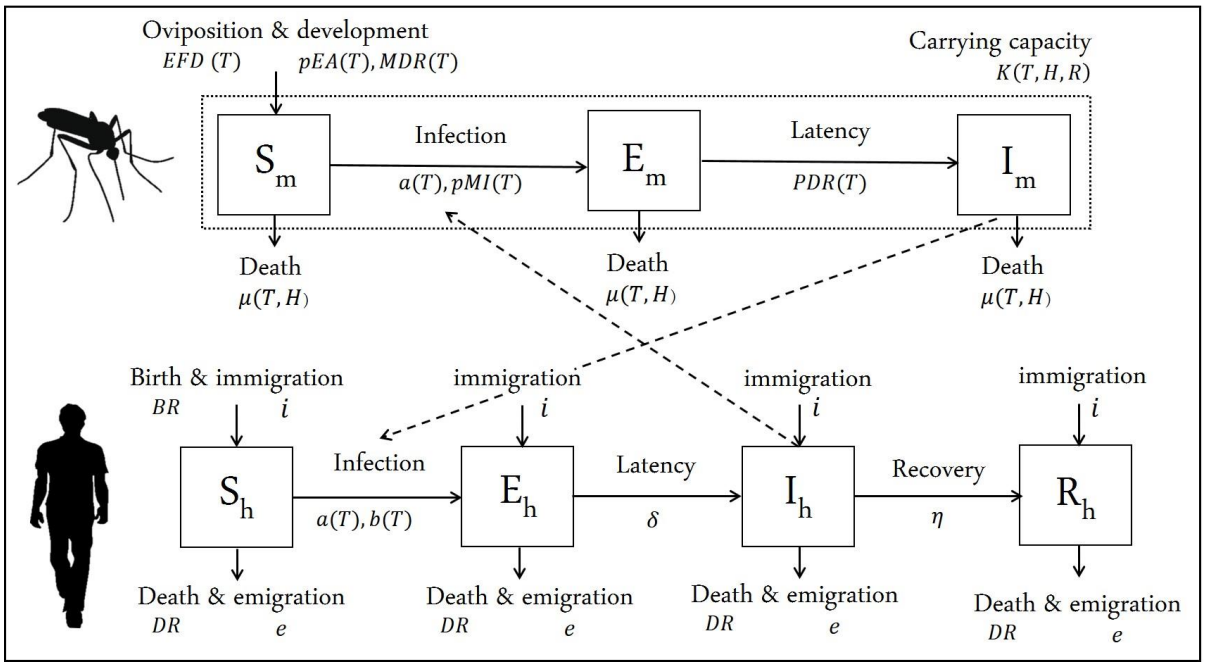

Figure 2: SEI-SEIR epidemiological model framework. The mosquito population is split among susceptible (S_m), exposed (E_m), and infectious (I_m) compartments (squares) and the human population is split among susceptible (S_h), exposed (E_h), infectious (I_h), and recovered (R_h) compartments. Solid arrows indicate the direction individuals can move between classes and dashed arrows indicate the direction of transmission. Transitions among compartments are labeled by the appropriate processes and corresponding rate parameters (see Methods for parameter definitions and more detail). Rate parameters with a T, H, and R are temperature-, humidity-, and rainfall-dependent, respectively. The total adult mosquito population (S_m, E_m, and I_m compartments; dotted rectangle) is maintained at an abundance less than or equal to the mosquito carrying capacity.

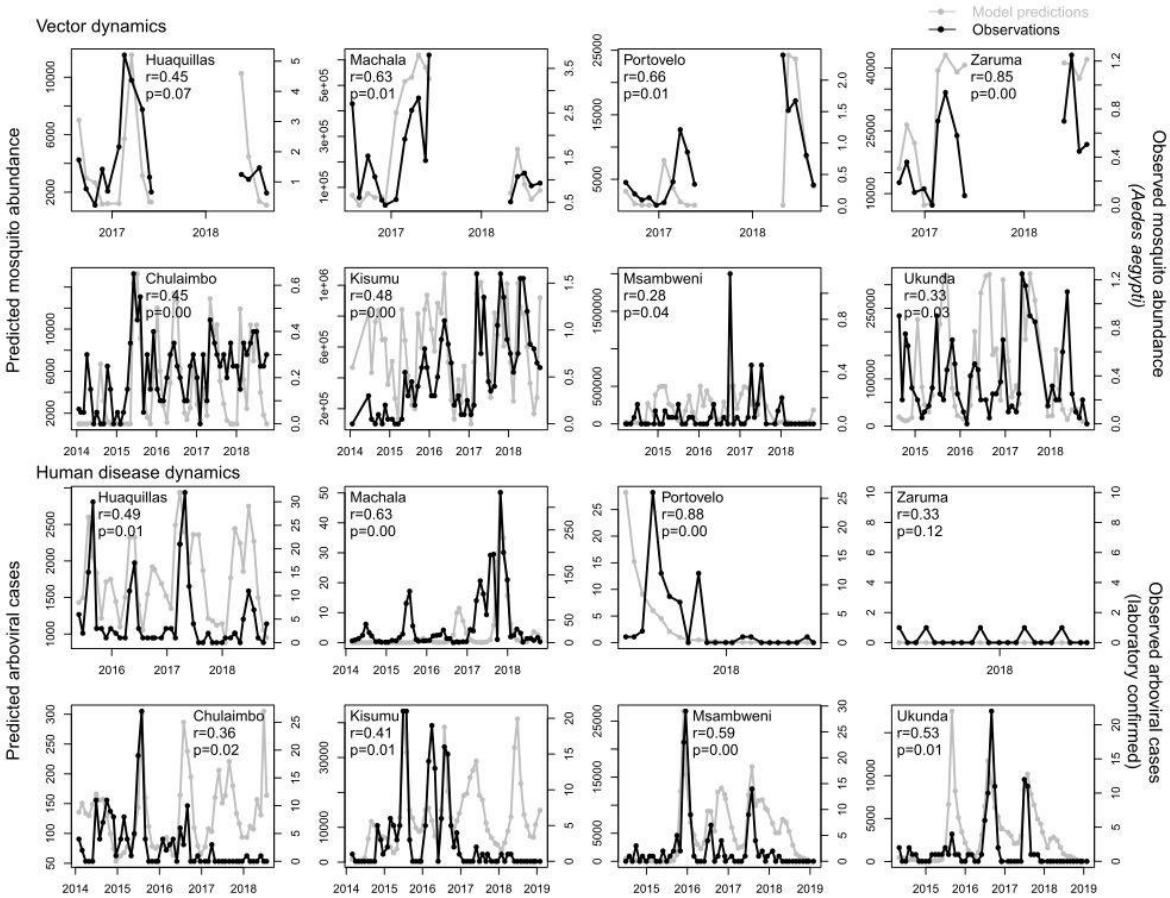

Figure 3: Model predicts vector and human disease dynamics with varying levels of accuracy across settings. Each plot shows the time series of SEI-SEIR model predictions (grey dots connected by grey lines) and field observations (black dots connected by black lines) for vector (top two rows) and human disease (bottom two rows) dynamics for each study site. The pairwise correlation (r) and adjusted p-value (p) are shown for each study site. We calculated observed mosquito abundances as the mean number of adult *Aedes aegypti* per house, month, year, and site. We calculated observed arboviral cases as the total number of laboratory-confirmed dengue (any serotype), chikungunya, and Zika cases per month, year, and site; six of the eight study sites only included dengue cases (see Methods). Ecuador sites are shown in the first and third rows

and Kenya sites in the second and fourth rows. We show uncertainty in model predictions in Figs. S1-2.

Table 2: Model predictions reflect a range of observed transmission dynamics when incorporating different rainfall functions and time lags across sites. For each study site, we calculated pairwise correlations between time series of field observations (*Aedes aegypti* abundances or arboviral cases) and time series of model predictions for the SEI-SEIR model with one of three rain functions for mosquito carrying capacity (Brière, Inverse, or Quadratic) and five time lags (0-4 months). This table shows specifications for the model (e.g., rain function and time lag) with the highest pairwise correlation value, r, for each study site and observation type (vectors or human disease cases), as well as the statistical significance of the correlation value compared with r = 0 (adjusted p-value) based on the Modified Chelton method [46] to account for autocorrelation.

	Vector dynamics				Human disease dynamics			
Site	Rain function	r	Adjusted p-value	Lag (months)	Rain function	r	Adjusted p-value	Lag (months)
Huaquillas, Ecuador	Brière	0.45	0.07	1	Inverse	0.49	0.01	2
Machala, Ecuador	Quadratic	0.63	0.01	0	Brière	0.63	0.00	4
Portovelo, Ecuador	Brière	0.66	0.01	1	Brière	0.88	0.00	3
Zaruma, Ecuador	Inverse	0.85	0.00	1	Inverse	0.33	0.12	0
Chulaimbo, Kenya	Inverse	0.45	0.00	1	Quadratic	0.36	0.02	4
Kisumu, Kenya	Brière	0.48	0.00	0	Inverse	0.41	0.01	4
Msambweni, Kenya	Inverse	0.28	0.04	0	Inverse	0.59	0.00	4
Ukunda, Kenya	Inverse	0.33	0.03	1	Inverse	0.53	0.01	4

We tested three hypothesized functional relationships between rainfall and mosquito carrying capacity in the SEI-SEIR model and five time lags between predictions and observations, and found that the rainfall function and time lag that correlated most strongly with field observations differed between mosquito abundance versus arboviral incidence and across sites (Table 2). The mechanistic relationship between rainfall and mosquito abundance is not well understood and is likely to vary based on the interaction between nonlinear effects of rainfall on immature vector habitat availability and human water storage activities. Therefore, we simulated disease dynamics for each site three times, using one of three hypothesized rainfall relationships (Brière, inverse, and quadratic; Fig. S3) in each SEI-SEIR model. We determined the best rainfall function and time lag for each site based on the highest pairwise correlation value between model predictions and observations. The model with the exponentially decreasing inverse rain function (Fig. S3c), which indicates that mosquito abundances peak when there is no or low rainfall (likely as a result of water storage practices) described observed mosquito and disease dynamics most often, especially in the Kenya sites (Table 2). The left-skewed unimodal Brière rainfall function (Fig. S3a), which indicates that mosquito abundances increase with increasing rainfall until some threshold where flushing occurs, described disease dynamics in some settings, particularly in the Ecuador sites. The symmetric unimodal quadratic rainfall function (Fig. S3b), which indicates that mosquito abundances peak with intermediate amounts of rainfall and are reduced with low and high rainfall values, described disease dynamics in the fewest settings. Interestingly, we did not find a single rainfall function that consistently described dynamics for mosquitoes or arboviral cases across study sites, or for both mosquitoes and arboviral cases within

individual study sites (Table 2). In contrast, we did find some consistency with time lags. The model best predicted mosquito abundances in the same month or one month in the future. In more than half of the sites, the model best predicted human disease cases four months in the future, and in almost all sites at least two months in the future (the exception is Zaruma, where very few arbovirus cases were reported during the study period and were likely due to importation rather than local transmission).

Factors that mediate disease dynamics predictability

Predictability of disease dynamics varied with demography, housing quality, and insecticide use. Although the sample size is small (N = 8 sites), we found that the SEI-SEIR model generally predicted vector dynamics better in sites with a smaller proportion of young children in the population, lower mean temperature, and a larger proportion of homes without window screens and made of cement (Fig. 4a-d; list of all factors assessed are provided in Table 1). Based on the range of mean temperatures at our study sites (22 – 28°C), our findings indicate that vector dynamics become less predictable as temperatures near the optimal temperature for transmission (29°C) predicted from a model of transmission parameterized with laboratory thermal response data (Fig. 5). This complements phenomenological models that have found the effect of temperature is minimized near the empirically derived thermal optima (Fig. 5). The model predicted human disease dynamics better in sites with lower annual rainfall and a larger proportion of homes that spray insecticide (Fig. 4e-f). Based on the range of rainfall functions supported by the SEI-SEIR model, combined with the finding that human disease dynamics become less predictable with increasing mean annual rainfall, we propose a

conceptual model for the complex and nonlinear response(s) of disease dynamics to rainfall (Fig. 6).

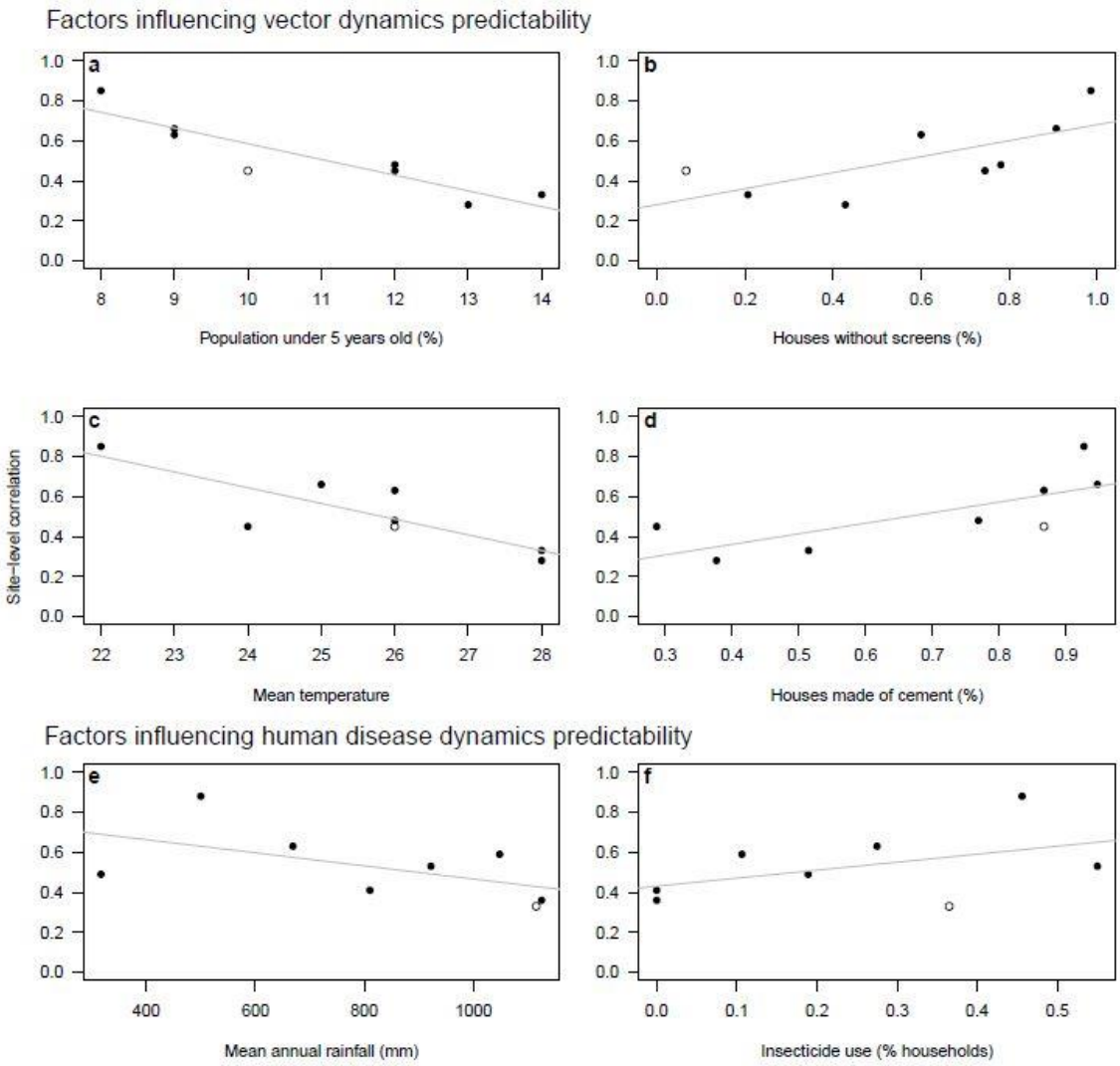

Figure 4: Demography, housing construction, climate, and insecticide use affect model predictive capacity. Factors that appear to influence the predictability of vector dynamics (top and center rows) include (a) proportion of the population under five years of age, (b) proportion of houses without window screens, (c) mean temperature, and (d) proportion of houses made with cement (walls and/or floors). Factors that may influence human disease dynamics (bottom row) include (e) mean annual rainfall and (f) proportion

of homes that use insecticide. In each plot, points indicate the pairwise correlation value for a single site. Filled circles indicate statistically significant pairwise correlations (adjusted p-value < 0.05) and open circles indicate non-statistically significant pairwise correlations (adjusted p-value ≥ 0.05). We display a grey linear regression line in each plot to aid visualization.

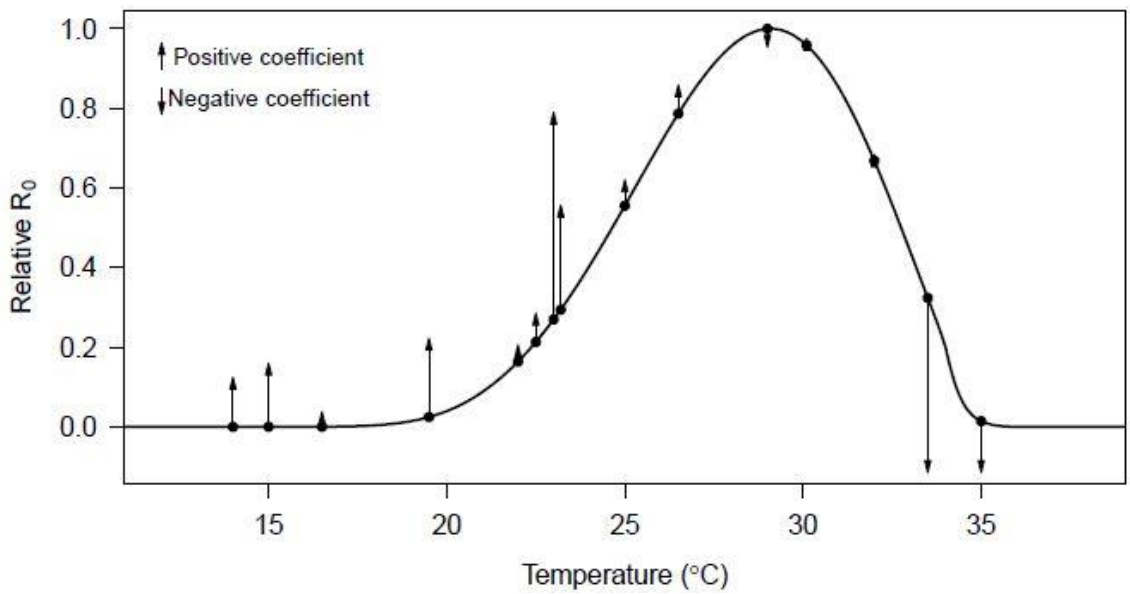

Figure 5: Independently predicted relative R_0 from an empirically derived model explains differences in the magnitude and direction of the effects of temperature on dengue transmission across varied settings from previous field studies. The black line shows the relative basic reproductive number (R_0, normalized to a 0-1 scale) plotted against temperature based on all temperature-dependent traits from [19] used in the SEI-SEIR model. Points indicate mean temperature values from previous field-based statistical analyses that related dengue cases with minimum, maximum, or mean ambient temperature; arrows correspond to the direction (up = positive, down = negative) and relative effect size of the temperature-dengue relationship based on coefficient values

from the following studies: [47,48,57,58,49–56]. See Methods and Table S1 for more detail. As expected, the largest observed positive effects of temperature occurred in the rapidly increasing portion of the R_0 curve (~22-25°C; consistent with findings in this study) and the largest observed negative effects occurred well above the predicted optimum, near the upper thermal limit (~33-35°C).

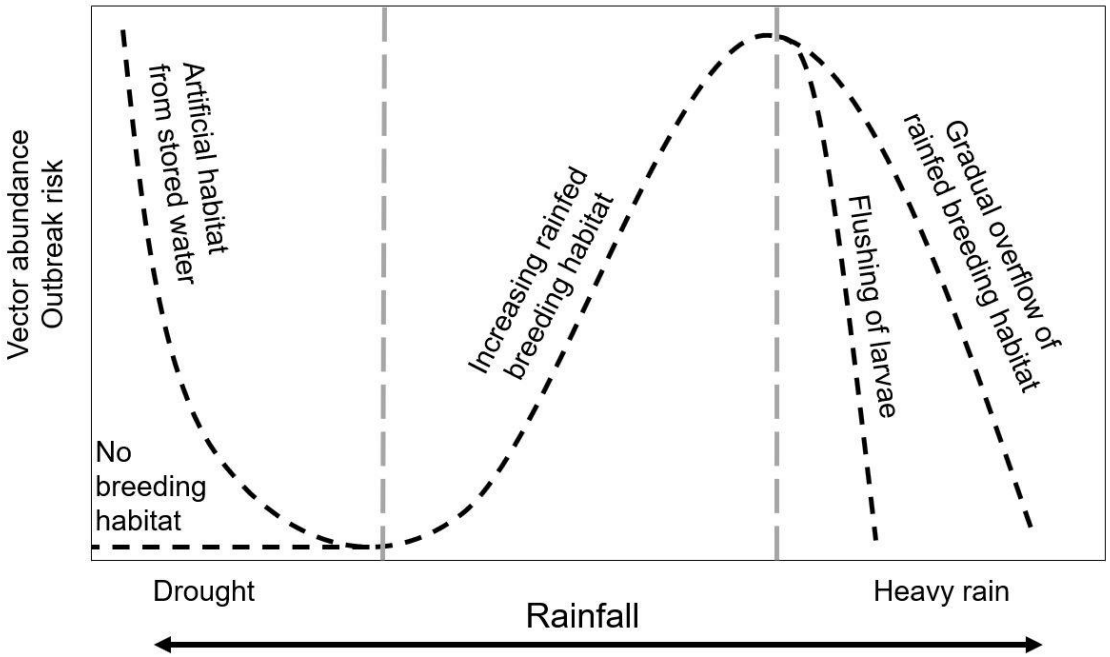

Figure 6: Conceptual model for nonlinear functional relationships between rainfall and vector abundance and arboviral outbreak risk. Dashed lines show multiple potential pathways for rainfall to affect transmission dynamics and include the functional relationships supported in this study. Labels indicate the hypothesized mechanisms along a gradient of rainfall. Adapted from [59].

Discussion:

Directly observing the influence of climate on species interactions and population dynamics is often challenging because of interacting and nonlinear relationships. Here, we directly and quantitatively connect laboratory-based climate relationships to observed mosquito and disease dynamics in the field, supporting the mechanistic role of climate in these disease systems. The trait-based modeling approach generated a range of disease dynamics, helping to reconcile seemingly context dependent effects (i.e., opposite conclusions about the magnitude and direction of effects; Fig. 5) of climate on arboviral transmission dynamics from the literature [7–12,47]. Our results highlight that we should not expect the same climate conditions and lags to be important in all settings, but that their combined, nonlinear effects can generally predict disease dynamics across different ecological and socio-economic settings (Table 2, Figs. 3, 5-6).

Although the model predicted important features of the temporal and spatial variation in vector and human disease dynamics, the accuracy of model predictions varied with some ecological and socio-economic factors such as demography, housing construction, and human behavior (Fig. 4). The model may have better predicted vector dynamics in locations with children under five years old for a variety of reasons, including because bottom-heavy demographic pyramids are often associated with lower socioeconomic status, because larger households may attract more mosquitoes, and/or because young children provide a consistent blood meal source in the home for day-biting mosquitoes. In addition to the demographic makeup of sites, housing construction within sites also seems to modify transmission dynamics: vector dynamics were less predictable in sites

with more window screens and houses made of cement (Fig. 4b,d). These results suggest that window screens may prevent mosquitoes from entering and biting people inside their homes, as indicated in some previous studies (e.g., [60]). Similarly, housing materials like cement that lower indoor temperature could artificially decrease climate suitability for mosquitoes, thereby decreasing the probability that mosquitoes will enter and bite people inside their homes. Despite incorporating all known temperature-dependent mosquito traits into the SEI-SEIR model, we still found vector dynamics became less predictable near the empirically derived thermal optima for arboviral transmission (Figs. 4c, 5). This finding may be associated with physiological or behavioral responses of mosquitoes to temperatures near their thermal safety margin [61,62] and/or humans modifying their environment (as described above) in locations optimal for transmission. Human disease dynamics were more predictable in sites with high levels of insecticide use. This somewhat counterintuitive result may arise because people are more likely to use vector control strategies in locations optimal for arboviral transmission, based on perceived risk from prior outbreaks, or because people are more likely to use insecticide where they frequently get bitten by mosquitoes.

Across our study sites, we found support for three hypothesized relationships between rainfall and mosquito carrying capacity as well as several time lags between model predictions and disease observations. Support for multiple rainfall functions could indicate that the effects of rainfall on immature habitat is highly heterogenous, which has been found in previous research in Ecuador [27] and Kenya [63]. Alternatively, the combination of multiple rainfall relationships and time lags could arise from nonlinear

and delayed effects of extreme climate such as droughts and floods. More specifically, we hypothesize that there may be multiple mechanistic relationships for the effects of rainfall on mosquito abundance and arboviral disease dynamics (Fig. 6), and they may act on different time scales. For example, previous research indicated that dengue outbreaks were more likely to occur four to five months after a drought and one month after excessive rainfall and a statistical model that incorporated these duel exposure-lag-response functions was highly effective at predicting dengue outbreaks in Barbados [64]. Further, if multiple rainfall relationships act in concert across varying time lags, this would help explain why many different time lags have been observed between rainfall and arboviral dynamics in previous studies [6,27,51,65–67].

Future research can build on this study to improve arboviral outbreak prediction. There were several factors that we did not include in this study, such as existing vector control programs, infrastructure, and preexisting immunity in the population. For instance, in Ecuador, factors such as distance to abandoned properties, interruptions in access to piped water, shaded patios, and use of vector control are known to influence arbovirus transmission [68], whereas in the study sites in Kenya, factors associated with arboviral transmission are less well studied and there are currently no widely used vector control or local arboviral surveillance programs employed. Future studies could further improve the model by incorporating human immune dynamics associated with interactions among different dengue serotypes [69] or cross-reactivity among viral antibodies [70], differential susceptibility across human age classes [71], and heterogeneity in contact rates between mosquitoes and people based on human behavior and movement [72,73].

Further, as experimental data becomes available for trait estimates specific to chikungunya and Zika, this model could be partitioned to model each arboviral disease individually. This is likely to be an important addition as the different arboviruses tend to peak in different years. There were not enough data for chikungunya and Zika cases in this study to formally test such patterns. This study provides strong evidence that a trait-based model, parameterized independently from field data, can predict a range of arboviral disease dynamics. Such mechanistic, climate-driven models will become increasingly important to support public health efforts in the face of novel climate regimes emerging due to climate change.

Materials and Methods:

Climate data

We collected *in situ* measurements of daily mean temperature, relative humidity, and rainfall at each study site and interpolated missing data where necessary. We used temperature and humidity measurements from HOBO loggers and rainfall measurements from rain gauges for sites in Kenya. We used temperature, humidity, and rainfall measurements from automatic weather stations operated by the National Institute of Meteorology and Hydrology in Ecuador. For Kenya, we interpolated missing temperature data from NOAA Global Surface Summary of the Day (Table S2, Fig. S4) and interpolated missing rainfall data from NOAA Climate Prediction Center Africa Rainfall Climatology dataset (Table S2, Fig. S5). For Ecuador, we interpolated missing temperature (Table S2, Fig. S4) and rainfall (Table S2, Fig. S5) data using the nearest study site where possible and otherwise based on long term mean values for the

corresponding Julian day. To interpolate missing data, we linearly regressed all measurements taken on the same day in two datasets and then used the linear model to interpolate temperature for the site with missing data based on the climate measurement from the secondary source for the date when the data was missing (Figs. S4-5). For rainfall, we first calculated a moving window of 14-day accumulated rainfall (following [74]) for each day before interpolation because modeled daily rainfall values are less reliable than accumulated rainfall over a two week period. We interpolated 14-day cumulative rainfall for any day with a missing rainfall value in the prior 14 days. For both Kenya and Ecuador, we interpolated missing relative humidity data based on long term mean values for the corresponding Julian day (Table S2). We then calculated the saturation vapor pressure deficit (SVPD) from temperature and humidity to use in the humidity function because previous research suggests SVPD is a more informative measure of the effect of humidity on mosquito survival compared with relative humidity [75]. To calculate SVPD, we first calculated the saturation vapor pressure as:

$$SVP = 610.7 * 10^{7.5*T/(273.3+T)} \quad (1)$$

where (T) is temperature in degrees Celsius. We then calculated SVPD (in kilopascals) as

$$SVPD = 1 - \frac{RH}{100} * SVP \quad (2)$$

where RH is relative humidity. The final dataset had no missing values for temperature (Fig. S6), rainfall (Fig. S7), and humidity (Fig. S8).

Vector surveys

We collected, counted, sexed, and classified mosquitoes by species, and aggregated the data to mean number of *Aedes aegypti* per house, month, year, and site to account for

differences in survey effort across months and sites. We collected adult mosquitoes using Prokopack aspirators [76]. In Ecuador, we collected mosquitoes from approximately 27 houses per site (range = 3-57 houses across four sites) every one-to-two weeks during three, four-month sampling periods between July 2016 and August 2018 (≈ 37 sampling weeks per site) to capture different parts of the transmission season. We aggregated the Ecuador vector data to monthly values (≈ 15 sampling months per site) to correspond with the temporal resolution of surveys in Kenya. In Kenya, we collected mosquitoes from approximately 20 houses per site (range = 1-47 houses across four sites) every month between January 2014 and October 2018 (≈ 54 sampling months per site). In Kenya, we also collected pupae, late instars, and early instars from containers with standing water around the home and collected eggs by setting ovitraps for an average of four days in and around each house monthly. We brought pupae, late and early instars, and eggs to the insectary and reared them to adulthood to classify individuals by sex and species. All mosquito traps capture a small portion of the true mosquito population; therefore, using consistent trapping methods at the same locations through time allows us to compare relative mosquito population dynamics across study sites rather than the absolute magnitude of mosquito abundances.

Arboviral surveys

For Ecuador, we analyzed laboratory-confirmed dengue, chikungunya, and Zika cases provided by the Ministry of Health (MoH) of Ecuador. The MoH collects serum samples from a subset of people with suspected arbovirus infections, and samples are tested at the National Public Health Research Institute by molecular diagnostics (RT-PCR) or

antibody tests (IgM ELISA for dengue), depending on the number of days of illness. Results are sent to the MoH Epidemiological Surveillance and Control National Directorate (SIVE Alerta system). Laboratory-confirmed dengue cases were available for all four sites from 2014 to 2018. Laboratory-confirmed chikungunya cases were available for Machala and Huaquillas from 2015 to 2018. Laboratory-confirmed Zika cases were available for Machala from 2016 to 2018.

For Kenya, we used laboratory-confirmed dengue cases aggregated by site and month between 2014 and 2018 collected in a passive surveillance study on childhood febrile illness in Kenya (NIH R01AI102918, PI: ADL). The study population consisted of 7,653 children less than 18 years of age with undifferentiated febrile illness. Children with fever enrolled in the study when attending outpatient care in one of the four study sites (Mbaka Oromo Health Centre in Chulaimbo, Obama Children's Hospital in Kisumu, Msambweni District Hospital in Msambweni, and Ukunda/Diani Health Center in Ukunda). Local health officers collected comprehensive clinical and demographic data and phlebotomy at the initial visit. We tested each child's blood for dengue viremia by molecular diagnostics (conventional PCR [77] or targeted multiplexed real-time PCR when available [78]), or serologic conversion between an initial and a follow up visit (IgG ELISA [79]).

SEI-SEIR model

We adapted an SEI-SEIR model parameterized for dengue transmission in *Ae. aegypti* mosquitoes [35] to simulate mosquito abundance and arboviral cases through time based on daily weather conditions in eight study locations. The model (equations 3-9; Fig. 2),

created independently from the observed data described above, allows mosquito life history traits and viral development rate to vary with temperature (T) following [35], mosquito carrying capacity to vary with accumulated 14-day rainfall (R) following [74], and mosquito mortality to vary with humidity (i.e., saturation vapor pressure deficit) (H) following [75].

$$\frac{dS_m}{dt} = \varphi(T,H) * \frac{1}{\mu(T,H)} * N_m * \left(1 - \frac{N_m}{K(T,R,H)}\right) - \left(a(T) * pMI(T) * \frac{I_h}{N_h} + \mu(T,H)\right) * S_m \quad (3)$$

$$\frac{dE_m}{dt} = a(T) * pMI(T) * \frac{I_h}{N_h} * S_m - \left(PDR(T) + \mu(T,H)\right) * E_m \quad (4)$$

$$\frac{dI_m}{dt} = PDR(T) * E_m - \mu(T,H) * I_m \quad (5)$$

$$\frac{dS_h}{dt} = -a(T) * b(T) * \frac{I_m}{N_h} * S_h + BR * S_h - DR * S_h + ie * N_h - ie * S_h \quad (6)$$

$$\frac{dE_h}{dt} = a(T) * b(T) * \frac{I_m}{N_h} * S_h - \delta * E_h - DR * E_h - ie * E_h \quad (7)$$

$$\frac{dI_h}{dt} = \delta * E_h - \eta * I_h - DR * I_h - ie * I_h \quad (8)$$

$$\frac{dR_h}{dt} = \eta * I_h - DR * R_h - ie * R_h \quad (9)$$

where

$$\varphi(T,H) = EFD(T) * pEA(T) * MDR(T) \quad (10)$$

The adult mosquito population (N_m) is separated into susceptible (S_m), exposed (E_m), and infectious (I_m) compartments and the human population (N_h) is separated into susceptible (S_h), exposed (E_h), infectious (I_h), and recovered (R_h) compartments (Fig. 2). Climate-independent model parameters (Table 3) include the intrinsic incubation period (δ), human infectivity period (η), birth rate (BR), death rate (DR), and immigration/emigration rate (ie). The temperature-dependent SEI-SEIR model was developed by Huber et al. [35] and allows mosquito life history traits and viral development rate to vary according to

thermal response curves fit from data derived in laboratory experiments conducted at constant temperatures (Table 3). The temperature-dependent traits include eggs laid per female per day (EFD), the probability of egg-to-adult survival (pEA), mosquito development rate (MDR), mosquito mortality rate (lifespan^{-1}; μ), biting rate (a), probability of mosquito infection per bite on an infectious host (pMI), parasite development rate (PDR), and probability of mosquito infectiousness given an infectious bite (b). We modified the mosquito mortality rate equation to vary as a function of temperature and humidity by fitting a spline model based on a pooled survival analysis of *Ae. aegypti* [75] (Fig. S9):

$$\mu(T,H) = \frac{1}{c*(T-T_0)*(T-T_m)} + (1-(0.01+2.01*H))*y \qquad H<1 \qquad (11)$$

$$\mu(T,H) = \frac{1}{c*(T-T_0)*(T-T_m)} + (1-(1.22+0.27*H))*y \qquad H\geq 1 \qquad (12)$$

where the rate constant (c), minimum temperature (T_0), and maximum temperature (T_m) equal -1.24, 16.63, and 31.85 respectively (Table 4), humidity (H) is the saturation vapor pressure deficit, and y is a scaling factor that we set to 0.005 and 0.01, respectively, to restrict mosquito mortality rates within the range of mortality rates estimated by other studies [19,75]. The linear humidity function has a steeper slope at lower humidity values (equation 11) compared with higher humidity values (equation 12) based on previous research [75] (Fig. S9).

We modeled adult mosquito carrying capacity, K, as a modified Arrhenius equation following [35,80]:

$$K(T,H,R) = \frac{EFD(T_0)*pEA(T_0)*MDR(T_0)*\mu(T_0,H_0)^{-1} - \mu(T_0,H_0)}{EFD(T_0)*pEA(T_0)*MDR(T_0)*\mu(T_0,H_0)^{-1}} * N_{m.max} \qquad (13)$$

$$* e^{\frac{-E_A*(T-T_0)^2}{\kappa_B*(T+273)*(T_0+273)}} * f(R)$$

with T_0 and H_0 set to the temperature and humidity where carrying capacity is greatest (i.e., physiological optimal conditions from laboratory experiments; 29°C and 6 kPA), $N_{m.max}$ set to the maximum possible mosquito abundance in a population (twice the human population size following [35]), and the Boltzmann constant, (K_B), is 8.617 x 10^{-5} eV/K. We set the activation energy, E_A, as 0.05 based on [35]. Since there were no experimental data from which to derive the functional response of mosquito carrying capacity across a gradient of rainfall values, we tested several functional relationships based on hypothesized biological relationships between freshwater availability and immature mosquito breeding habitat, modeling the effect of rainfall on carrying capacity, *f*(*R*), as either:

$$f(R_{\text{Brière}}) = c * R * (R - R_{min}) * \sqrt{(R_{max} - R)} * y \quad (14)$$

$$f(R_{Quadratic}) = c * (R - R_{min}) * (R - R_{max}) * y \quad (15)$$

$$f(R_{\text{Inverse}}) = \frac{1}{R} \quad (16)$$

where minimum rainfall (R_{min}) equaled 1 mm and maximum rainfall (R_{max}) equaled 123 mm based on the high probability of flushing [26]. The quadratic function is similar to the rainfall function found in [26] and the inverse function is based on the rainfall function used in [74]. We used rate constants (c) of 7.86e^{-5} and -5.99e^{-3} for the Brière and quadratic functions respectively, based on rate constants for other parameters with similar functional forms (Table 4). We scaled the Brière and quadratic functions by y (0. 268 and 0.045, respectively) so that the maximum carrying capacity was approximately equal across all three functions.

Table 3: Values of temperature-invariant parameters used in the model. We derived daily birth and death rates in the model by dividing the per capita birth and death rates by 360 days. The World Bank Open Data can be found at https://data.worldbank.org/.

Parameter	Definition	Value	Source
δ^{-1}	Intrinsic incubation period (days)	5.9	[35]
η^{-1}	Human infectivity period (days)	5.0	[35]
BR	Annual birth rate (per 1000 people)	31.782 (Ecuador) 20.175 (Kenya)	The World Bank Open Data
DR	Annual death rate (per 1000 people)	5.284 (Ecuador) 5.121 (Kenya)	The World Bank Open Data
ie	Immigration/emigration rate	0.01	Expert opinion

Table 4: Fitted thermal responses for *Ae. aegypti* life history traits. Traits were fit to a Brière [$cT(T-T_0)(T_m-T)^{\frac{1}{2}}$] or a quadratic [$c(T-T_m)(T-T_0)$] function where T represents temperature. T_0 and T_m are the critical thermal minimum and maximum, respectively, and c is the rate constant. Thermal responses were fit by [19] and also used in [35]. Parasite development rate was measured as the virus extrinsic incubation rate.

Trait	Definition	Function	c	T_0	T_m
a	Biting rate (day^{-1})	Brière	2.71×10^{-04}	14.67	41.00
EFD	Eggs laid per female per day	Brière	2.08×10^{-02}	14.06	32.03
pEA	Probability of mosquito egg-to-adult survival	Quadratic	-3.36×10^{-03}	7.68	38.31
MDR	Mosquito egg-to-adult development rate (day^{-1})	Brière	1.49×10^{-04}	15.12	37.67
Lf	Adult mosquito lifespan (days)	Quadratic	-1.24	16.63	31.85
b	Probability of mosquito infectiousness	Brière	9.86×10^{-04}	12.05	32.79
pMI	Probability of mosquito infection	Brière	5.23×10^{-04}	1.51	34.74
PDR	Parasite development rate (day^{-1})	Brière	1.04×10^{-04}	11.50	38.97

To initiate the model, we used site-specific values for human population size and randomly selected one set of values for all sites for the proportion of mosquitoes and humans in each compartment. For Ecuador, we used population estimates from official population projections produced by Proyección de la Población Ecuatoriana, por años calendario, según cantones 2010-2020 (https://www.ecuadorencifras.gob.ec/proyecciones-poblacionales/) with population sizes of 57,366, 279,887, 13,673, and 25,615 for Huaquillas, Machala, Portovelo, and Zaruma, respectively, based on 2017 projections. For Kenya, we estimated the population sizes

served by each outpatient care facility by creating a polygon around all the geolocations of study participants' homes enrolled at each outpatient care facility and summed population count data from NASA's Socioeconomic Data and Applications Center Gridded Population of the World v4 (https://doi.org/10.7927/H4JW8BX5) within each polygon using ArcGIS v 10.4.1. We estimated population sizes of 7,304, 547,557, 240,698, and 154,048 for Chulaimbo, Kisumu, Msambweni, and Ukunda, respectively. We used the following values as the initial proportion of mosquitoes and humans in each model compartment: $S_m = 0.22$, $E_m = 0.29$, $I_m = 0.49$, $S_h = 0.58$, $E_h = 0.22$, $I_h = 0.00$, and $R_h = 0.20$. We determined that the model was invariant to initial proportion values after a short burn-in period (90 days) based on a sensitivity analysis (Fig. S10); therefore, we randomly selected one set of initial proportion values from the sensitivity analysis for all the model simulations. We also determined that the temporal trajectories of model dynamics did not change when we varied the critical thermal minimum, maximum, and rate constants (Table 4) for *Aedes aegypti* life history traits (Fig. S1-2).

We ran all model simulations using the deSolve package in R statistical software v 3.5.3 [81]. Model codes are available at https://github.com/jms5151/SEI-SEIR_Arboviruses.

Model validation

To validate the SEI-SEIR model, we calculated pairwise correlations with an adjusted p-value to account for autocorrelation for each site. For the pairwise correlations, we used the ccf function in base R [81] to calculate correlations between the two times series of model predictions and observations with 0, 1, 2, 3, and 4-month lags. We then calculated

an adjusted p-value using the Modified Chelton method [46] to adjust the null hypothesis test of sample correlation between autocorrelated time series. To assess predictions and observations for vector dynamics for each site, we compared monthly time series of the total predicted mosquito population from the SEI-SEIR model with the monthly time series of mean number of *Aedes aegypti* (per house). We followed the same procedure to compare model predictions with other mosquito life stages for sites in Kenya. Similarly, to compare predictions and observations for human disease dynamics for each site, we compared monthly times series of predicted infected individuals from the SEI-SEIR model with the monthly time series of total laboratory-confirmed arboviral cases.

Comparison of R_0 with prior studies

We collected effect sizes of temperature on dengue incidence from 12 peer-reviewed studies from the literature (Table S1). We selected studies with mean temperatures across the predicted temperature range where arboviral transmission can occur. We scaled the coefficient values to visualize the relative effect of temperature across studies given that the original analyses were conducted with different temperature metrics and across different temperature ranges. We provide additional information and sources in Table S1.

Acknowledgements: JMC, ADL, EFL, and EAM were supported by a Stanford Woods Institute for the Environment – Environmental Ventures Program grant (PIs: EAM, ADL, and EFL). EAM was also supported by a Hellman Faculty Fellowship and a Terman Award. ADL, BAN, FMM, ENGS, MSS, ARK, RD, AA, and HNN were supported by a National Institutes of Health R01 grant (AI102918; PI: ADL). EAM, AMSI, and SJR

were supported by a National Science Foundation Ecology and Evolution of Infectious Diseases grant (DEB-1518681) and AMSI and SJR were also supported by an NSF DEB RAPID grant (1641145). EAM was supported by a National Institute of General Medical Sciences Maximizing Investigators' Research Award grant (1R35GM133439-01). We thank Cat Lippi for assistance with formatting household quality survey data from Ecuador.

Author contributions: EAM, ADL, EFL, and JMC conceived of project. JMC conducted analyses and wrote manuscript. EAM, ADL, EFL, and AMSI secured funding for the project. BNN, FMM, EBA, AA, MJBC, RD, FHH, RM, and HNN collected data. ENGS and MMS conducted laboratory analyses. ARK, SJR, and RS processed data. All authors revised and approved of the manuscript.

References:

1. Ockendon N, Baker DJ, Carr JA, White EC, Almond REA, Amano T, et al. Mechanisms underpinning climatic impacts on natural populations: altered species interactions are more important than direct effects. Glob Chang Biol. 2014;20: 2221–2229. doi:10.1111/gcb.12559
2. Boggs CL, Inouye DW. A single climate driver has direct and indirect effects on insect population dynamics. Ecol Lett. 2012;15: 502–508. doi:10.1111/j.1461-0248.2012.01766.x
3. Burkett VR, Wilcox DA, Stottlemyer R, Barrow W, Fagre D, Baron J, et al. Nonlinear dynamics in ecosystem response to climatic change: Case studies and policy implications. Ecol Complex. 2005;2: 357–394. doi:10.1016/j.ecocom.2005.04.010
4. Molnár PK, Sckrabulis JP, Altman KA, Raffel TR. Thermal Performance Curves and the Metabolic Theory of Ecology—A Practical Guide to Models and Experiments for Parasitologists. J Parasitol. 2017;103. doi:10.1645/16-148
5. Hortion J, Mutuku FM, Eyherabide AL, Vu DM, Boothroyd DB, Grossi-Soyster EN, et al. Acute Flavivirus and Alphavirus Infections among Children in Two Different Areas of Kenya, 2015. Am J Trop Med Hyg. 2019;100: 170–173. doi:10.4269/ajtmh.18-0297
6. Stewart-Ibarra AM, Lowe R. Climate and Non-Climate Drivers of Dengue Epidemics in Southern Coastal Ecuador. Am J Trop Med Hyg. 2013;88: 971–981. doi:10.4269/ajtmh.12-0478
7. Jury MR. Climate influence on dengue epidemics in Puerto Rico. Int J Environ

Health Res. 2008;18: 323–334. doi:10.1080/09603120701849836

8. Campbell KM, Haldeman K, Lehnig C, Munayco C V., Halsey ES, Laguna-Torres VA, et al. Weather Regulates Location, Timing, and Intensity of Dengue Virus Transmission between Humans and Mosquitoes. Michael E, editor. PLoS Negl Trop Dis. 2015;9: e0003957. doi:10.1371/journal.pntd.0003957

9. Adde A, Roucou P, Mangeas M, Ardillon V, Desenclos J-C, Rousset D, et al. Predicting Dengue Fever Outbreaks in French Guiana Using Climate Indicators. Scarpino S V., editor. PLoS Negl Trop Dis. 2016;10: e0004681. doi:10.1371/journal.pntd.0004681

10. Dhimal M, Gautam I, Joshi HD, O'Hara RB, Ahrens B, Kuch U, et al. Risk Factors for the Presence of Chikungunya and Dengue Vectors (Aedes aegypti and Aedes albopictus), Their Altitudinal Distribution and Climatic Determinants of Their Abundance in Central Nepal. Turell MJ, editor. PLoS Negl Trop Dis. 2015;9: e0003545. doi:10.1371/journal.pntd.0003545

11. Descloux E, Mangeas M, Menkes CE, Lengaigne M, Leroy A, Tehei T, et al. Climate-Based Models for Understanding and Forecasting Dengue Epidemics. Anyamba A, editor. PLoS Negl Trop Dis. 2012;6: e1470. doi:10.1371/journal.pntd.0001470

12. Aswi A, Cramb SM, Moraga P, Mengersen K. Epidemiology and Infection Bayesian spatial and spatio-temporal approaches to modelling dengue fever: a systematic review. Epidemiol Infect. 2018;147. doi:10.1017/S0950268818002807

13. Johansson MA, Apfeldorf KM, Dobson S, Devita J, Buczak AL, Baugher B, et al. An open challenge to advance probabilistic forecasting for dengue epidemics. Proc

Natl Acad Sci. 2019; 201909865. doi:10.1073/pnas.1909865116

14. Michael E, Singh BK, Mayala BK, Smith ME, Hampton S, Nabrzyski J. Continental-scale, data-driven predictive assessment of eliminating the vector-borne disease, lymphatic filariasis, in sub-Saharan Africa by 2020. BMC Med. 2017;15: 176. doi:10.1186/s12916-017-0933-2

15. Smith T, Maire N, Ross A, Penny M, Chitnis N, Schapira A, et al. Towards a comprehensive simulation model of malaria epidemiology and control. Parasitology. 2008. pp. 1507–1516. doi:10.1017/S0031182008000371

16. Ryan SJ, Carlson CJ, Mordecai EA, Johnson LR. Global expansion and redistribution of Aedes-borne virus transmission risk with climate change. Han BA, editor. PLoS Negl Trop Dis. 2019;13: e0007213. doi:10.1371/journal.pntd.0007213

17. Kraemer MU, Sinka ME, Duda KA, Mylne AQ, Shearer FM, Barker CM, et al. The global distribution of the arbovirus vectors *Aedes aegypti* and *Ae. albopictus*. Elife. 2015;4. doi:10.7554/eLife.08347

18. Powell JR, Tabachnick WJ, Powell JR, Tabachnick WJ. History of domestication and spread of Aedes aegypti - A Review. Mem Inst Oswaldo Cruz. 2013;108: 11–17. doi:10.1590/0074-0276130395

19. Mordecai EA, Cohen JM, Evans M V., Gudapati P, Johnson LR, Lippi CA, et al. Detecting the impact of temperature on transmission of Zika, dengue, and chikungunya using mechanistic models. Althouse B, editor. PLoS Negl Trop Dis. 2017;11: e0005568. doi:10.1371/journal.pntd.0005568

20. Shocket MS, Ryan SJ, Mordecai EA. Temperature explains broad patterns of Ross

River virus transmission. Elife. 2018; doi:10.7554/eLife.37762.001

21. Paull SH, Horton DE, Ashfaq M, Rastogi D, Kramer LD, Diffenbaugh NS, et al. Drought and immunity determine the intensity of West Nile virus epidemics and climate change impacts. Proc R Soc B Biol Sci. 2017;284: 20162078. doi:10.1098/rspb.2016.2078

22. Costa EAP de A, Santos EM de M, Correia JC, Albuquerque CMR de. Impact of small variations in temperature and humidity on the reproductive activity and survival of Aedes aegypti (Diptera, Culicidae). Rev Bras Entomol. 2010;54: 488–493. doi:10.1590/S0085-56262010000300021

23. Gaaboub IA, El-Sawaf SK, El-Latif MA. Effect of Different Relative Humidities and Temperatures on Egg-Production and Longevity of Adults of Anopheles (Myzomyia) pharoensis Theob.1. Zeitschrift für Angew Entomol. 2009;67: 88–94. doi:10.1111/j.1439-0418.1971.tb02098.x

24. Koenraadt CJM, Harrington LC. Flushing Effect of Rain on Container-Inhabiting Mosquitoes Aedes aegypti and Culex pipiens (Diptera: Culicidae). J Med Entomol. 2009;45: 28–35. doi:10.1603/0022-2585(2008)45[28:FEOROC]2.0.CO;2

25. Paaijmans KP, Wandago MO, Githeko AK, Takken W, Vulule J. Unexpected High Losses of Anopheles gambiae Larvae Due to Rainfall. Carter D, editor. PLoS One. 2007;2: e1146. doi:10.1371/journal.pone.0001146

26. Benedum CM, Seidahmed OME, Eltahir EAB, Markuzon N. Statistical modeling of the effect of rainfall flushing on dengue transmission in Singapore. Reiner RC, editor. PLoS Negl Trop Dis. 2018;12: e0006935. doi:10.1371/journal.pntd.0006935

27. Stewart Ibarra AM, Ryan SJ, Beltrán E, Mejía R, Silva M, Muñoz Á. Dengue Vector Dynamics (Aedes aegypti) Influenced by Climate and Social Factors in Ecuador: Implications for Targeted Control. Mores CN, editor. PLoS One. 2013;8: e78263. doi:10.1371/journal.pone.0078263

28. Pontes RJ, Spielman A, Oliveira-Lima JW, Hodgson JC, Freeman J. Vector densities that potentiate dengue outbreaks in a Brazilian city. Am J Trop Med Hyg. 2000;62: 378–383. doi:10.4269/ajtmh.2000.62.378

29. Anyamba A, Linthicum KJ, Small JL, Collins KM, Tucker CJ, Pak EW, et al. Climate Teleconnections and Recent Patterns of Human and Animal Disease Outbreaks. Zhou X-N, editor. PLoS Negl Trop Dis. 2012;6: e1465. doi:10.1371/journal.pntd.0001465

30. Lourenço J, Recker M. The 2012 Madeira Dengue Outbreak: Epidemiological Determinants and Future Epidemic Potential. Scarpino S V., editor. PLoS Negl Trop Dis. 2014;8: e3083. doi:10.1371/journal.pntd.0003083

31. Li R, Xu L, Bjørnstad ON, Liu K, Song T, Chen A, et al. Climate-driven variation in mosquito density predicts the spatiotemporal dynamics of dengue. Proc Natl Acad Sci. 2019;119: 3624–3629. doi:10.1073/PNAS.1806094116

32. Wang X, Tang S, Cheke RA. A stage structured mosquito model incorporating effects of precipitation and daily temperature fluctuations. J Theor Biol. 2016;411: 27–36. doi:10.1016/j.jtbi.2016.09.015

33. Siraj AS, Oidtman RJ, Huber JH, Kraemer MUG, Brady OJ, Johansson MA, et al. Temperature modulates dengue virus epidemic growth rates through its effects on reproduction numbers and generation intervals. Althouse B, editor. PLoS Negl

Trop Dis. 2017;11: e0005797. doi:10.1371/journal.pntd.0005797

34. Oidtman RJ, Lai S, Huang Z, Yang J, Siraj AS, Reiner RC, et al. Inter-annual variation in seasonal dengue epidemics driven by multiple interacting factors in Guangzhou, China. Nat Commun. 2019;10. doi:10.1038/s41467-019-09035-x

35. Huber JH, Childs ML, Caldwell JM, Mordecai EA. Seasonal temperature variation influences climate suitability for dengue, chikungunya, and Zika transmission. Althouse B, editor. PLoS Negl Trop Dis. 2018;12: e0006451. doi:10.1371/journal.pntd.0006451

36. Stewart-Ibarra AM, Muñoz ÁG, Ryan SJ, Ayala EB, Borbor-Cordova MJ, Finkelstein JL, et al. Spatiotemporal clustering, climate periodicity, and social-ecological risk factors for dengue during an outbreak in Machala, Ecuador, in 2010. BMC Infect Dis. 2014;14: 610. doi:10.1186/s12879-014-0610-4

37. Agha SB, Tchouassi DP, Turell MJ, Bastos ADS, Sang R. Entomological assessment of dengue virus transmission risk in three urban areas of Kenya. Reiner RC, editor. PLoS Negl Trop Dis. 2019;13: e0007686. doi:10.1371/journal.pntd.0007686

38. Agha SB, Tchouassi DP, Bastos ADS, Sang R. Dengue and yellow fever virus vectors: seasonal abundance, diversity and resting preferences in three Kenyan cities. Parasit Vectors. 2017;10: 628. doi:10.1186/s13071-017-2598-2

39. Chretien J-P, Anyamba A, Bedno SA, Breiman RF, Sang R, Sergon K, et al. Drought-Associated Chikungunya Emergence Along Coastal East Africa. Am J Trop Med Hyg. 2007;76: 405–407. doi:10.4269/ajtmh.2007.76.405

40. Vu DM, Mutai N, Heath CJ, Vulule JM, Mutuku FM, Ndenga BA, et al.

Unrecognized Dengue Virus Infections in Children, Western Kenya, 2014-2015. Emerg Infect Dis. 2017;23: 1915–1917. doi:10.3201/eid2311.170807

41. Gubler DJ, Nalim S, Saroso JS, Saipan H, Tan R. Variation in Susceptibility to Oral Infection with Dengue Viruses among Geographic Strains of Aedes Aegypti *. Am J Trop Med Hyg. 1979;28: 1045–1052. doi:10.4269/ajtmh.1979.28.1045

42. Xavier-Carvalho C, Chester Cardoso C, de Souza Kehdya F, Guilherme Pacheco A, Ozório Moraesa M. Host genetics and dengue fever. Infect Genet Evol. 2017;56: 99–110. doi:10.1016/J.MEEGID.2017.11.009

43. Román MO, Wang Z, Sun Q, Kalb V, Miller SD, Molthan A, et al. NASA's Black Marble nighttime lights product suite. Remote Sens Environ. 2018;210: 113–143. doi:10.1016/j.rse.2018.03.017

44. Didan K, Barreto Munoz A, Solano R, Huete A. MODIS Vegetation Index User's Guide (MOD13 Series) [Internet]. Available: http://vip.arizona.edu

45. Sulla-Menashe D, Friedl MA. User Guide to Collection 6 MODIS Land Cover (MCD12Q1 and MCD12C1) Product. 2018; doi:10.5067/MODIS/MCD12Q1

46. Pyper BJ, Peterman RM. Comparison of methods to account for autocorrelation in correlation analyses of fish data. Can J Fish Aquat Sci. 1998;55: 2127–2140. doi:10.1139/f98-104

47. Hurtado-Daz M, Riojas-Rodrguez H, Rothenberg S, Gomez-Dantes H, Cifuentes E. Impact of climate variability on the incidence of dengue in Mexico. Trop Med Int Heal. 2007;12. doi:10.1111/j.1365-3156.2007.01930.x

48. Colón-González FJ, Bentham G, Lake IR. Climate Variability and Dengue Fever in Warm and Humid Mexico. Am J Trop Med Hyg. 2011;84: 757–763.

doi:10.4269/ajtmh.2011.10-0609

49. Wang C, Jiang B, Fan J, Wang F, Liu Q. A Study of the Dengue Epidemic and Meteorological Factors in Guangzhou, China, by Using a Zero-Inflated Poisson Regression Model. Asia Pacific J Public Heal. 2014;26: 48–57. doi:10.1177/1010539513490195

50. Minh An DT, Rocklöv J. Epidemiology of dengue fever in Hanoi from 2002 to 2010 and its meteorological determinants. Glob Health Action. 2014;7: 23074. doi:10.3402/gha.v7.23074

51. Laureano-Rosario AE, Garcia-Rejon JE, Gomez-Carro S, Farfan-Ale JA, Muller-Kargera FE. Modelling dengue fever risk in the State of Yucatan, Mexico using regional-scale satellite-derived sea surface temperature. Acta Trop. 2017;172: 50–57. doi:10.1016/j.actatropica.2017.04.017

52. Wu P-C, Guoa H-R, Lung S-C, Lin C-Y, Su H-J. Weather as an effective predictor for occurrence of dengue fever in Taiwan. Acta Trop. 2007;103: 50–57. doi:10.1016/j.actatropica.2007.05.014

53. Karim MN, Munshi SU, Anwar N, Alam MS. Climatic factors influencing dengue cases in Dhaka city: a model for dengue prediction. Indian J Med Res. 2012;136: 32–9. Available: http://www.ncbi.nlm.nih.gov/pubmed/22885261

54. Nakhapakorn K, Tripathi N. An information value based analysis of physical and climatic factors affecting dengue fever and dengue haemorrhagic fever incidence. Int J Health Geogr. 2005;4: 13. doi:10.1186/1476-072X-4-13

55. Gharbi M, Quenel P, Gustave J, Cassadou S, Ruche G La, Girdary L, et al. Time series analysis of dengue incidence in Guadeloupe, French West Indies:

Forecasting models using climate variables as predictors. BMC Infect Dis. 2011;11: 166. doi:10.1186/1471-2334-11-166

56. Sharmin S, Glass K, Viennet E, Harley D. Interaction of Mean Temperature and Daily Fluctuation Influences Dengue Incidence in Dhaka, Bangladesh. Kasper M, editor. PLoS Negl Trop Dis. 2015;9: e0003901. doi:10.1371/journal.pntd.0003901

57. Sriprom M, Chalvet-Monfray K, Chaimane T, Vongsawat K, Bicout DJ. Monthly district level risk of dengue occurrences in Sakon Nakhon Province, Thailand. Sci Total Environ. 2010;408: 5521–5528. doi:10.1016/J.SCITOTENV.2010.08.024

58. Martínez-Bello D, López-Quílez A, Prieto AT. Spatiotemporal modeling of relative risk of dengue disease in Colombia. Stoch Environ Res Risk Assess. 2018;32: 1587–1601. doi:10.1007/s00477-017-1461-5

59. Shocket MS, Anderson CB, Caldwell JM, Childs ML, Han S, Harris M, et al. Environmental drivers of vector-borne disease. Population Biology of Vector-borne Diseases. Oxford University Press;

60. Ko Y-C, Chen M-J, Yeh S-M. The Predisposing and Protective Factors against Dengue Virus Transmission by Mosquito Vector. Am J Epidemiol. 1992;136: 214–220. doi:10.1093/oxfordjournals.aje.a116487

61. Mordecai EA, Caldwell JM, Grossman MK, Lippi CA, Johnson LR, Neira M, et al. Thermal biology of mosquito-borne disease. Byers J (Jeb), editor. Ecol Lett. 2019; ele.13335. doi:10.1111/ele.13335

62. Carrington LB, Armijos MV, Lambrechts L, Barker CM, Scott TW. Effects of Fluctuating Daily Temperatures at Critical Thermal Extremes on Aedes aegypti Life-History Traits. PLoS One. 2013;8. doi:10.1371/journal.pone.0058824

63. Ngugi HN, Mutuku FM, Ndenga BA, Musunzaji PS, Mbakaya JO, Aswani P, et al. Characterization and productivity profiles of Aedes aegypti (L.) breeding habitats across rural and urban landscapes in western and coastal Kenya. Parasit Vectors. 2017;10: 331. doi:10.1186/s13071-017-2271-9

64. Lowe R, Gasparrini A, Van Meerbeeck CJ, Lippi CA, Mahon R, Trotman AR, et al. Nonlinear and delayed impacts of climate on dengue risk in Barbados: A modelling study. PLoS Med. 2018;15. doi:10.1371/journal.pmed.1002613

65. Li C, Wang X, Wu X, Liu J, Ji D, Du J. Modeling and projection of dengue fever cases in Guangzhou based on variation of weather factors. Sci Total Environ. 2017;605–606: 867–873. doi:10.1016/j.scitotenv.2017.06.181

66. Li CF, Lim TW, Han LL, Fang R. Rainfall, abundance of Aedes aegypti and dengue infection in Selangor, Malaysia. Southeast Asian J Trop Med Public Health. 1985;16: 560–8. Available: http://www.ncbi.nlm.nih.gov/pubmed/3835698

67. Johansson MA, Dominici F, Glass GE. Local and Global Effects of Climate on Dengue Transmission in Puerto Rico. Massad E, editor. PLoS Negl Trop Dis. 2009;3: e382. doi:10.1371/journal.pntd.0000382

68. Kenneson A, Beltrán-Ayala E, Borbor-Cordova MJ, Polhemus ME, Ryan SJ, Endy TP, et al. Social-ecological factors and preventive actions decrease the risk of dengue infection at the household-level: Results from a prospective dengue surveillance study in Machala, Ecuador. Messer WB, editor. PLoS Negl Trop Dis. 2017;11: e0006150. doi:10.1371/journal.pntd.0006150

69. Reich NG, Shrestha S, King AA, Rohani P, Lessler J, Kalayanarooj S, et al. Interactions between serotypes of dengue highlight epidemiological impact of

cross-immunity. J R Soc Interface. 2013;10: 20130414. doi:10.1098/rsif.2013.0414

70. Wen J, Elong Ngono A, Regla-Nava JA, Kim K, Gorman MJ, Diamond MS, et al. Dengue virus-reactive CD8+ T cells mediate cross-protection against subsequent Zika virus challenge. Nat Commun. 2017;8: 1459. doi:10.1038/s41467-017-01669-z

71. Rodriguez-Barraquer I, Salje H, Cummings DA. Opportunities for improved surveillance and control of dengue from age-specific case data. Elife. 2019;8. doi:10.7554/eLife.45474

72. Stoddard ST, Forshey BM, Morrison AC, Paz-Soldan VA, Vazquez-Prokopec GM, Astete H, et al. House-to-house human movement drives dengue virus transmission. Proc Natl Acad Sci U S A. 2013;110: 994–999. doi:10.1073/pnas.1213349110

73. Wesolowski A, Qureshi T, Boni MF, Sundsøy PR, Johansson MA, Rasheed SB, et al. Impact of human mobility on the emergence of dengue epidemics in Pakistan. Proc Natl Acad Sci. 2015;112: 11887–11892. doi:10.1073/pnas.1504964112

74. Vaidya A, Bravo-Salgado AD, Mikler AR. Modeling climate-dependent population dynamics of mosquitoes to guide public health policies. Proc 5th ACM Conf Bioinformatics, Comput Biol Heal Informatics - BCB ’14. 2014; 380–389. doi:10.1145/2649387.2649415

75. Schmidt CA, Comeau G, Monaghan AJ, Williamson DJ, Ernst KC. Effects of desiccation stress on adult female longevity in Aedes aegypti and Ae. albopictus (Diptera: Culicidae): results of a systematic review and pooled survival analysis.

Parasit Vectors. 2018;11: 267. doi:10.1186/s13071-018-2808-6

76. Vazquez-Prokopec GM, Galvin WA, Kelly R, Kitron U. A New, Cost-Effective, Battery-Powered Aspirator for Adult Mosquito Collections. J Med Entomol. 2009;46: 1256–1259. doi:10.1603/033.046.0602

77. Waggoner JJ, Gresh L, Mohamed-Hadley A, Ballesteros G, Davila MJV, Tellez Y, et al. Single-Reaction Multiplex Reverse Transcription PCR for Detection of Zika, Chikungunya, and Dengue Viruses. Emerg Infect Dis. 2016;22: 1295–7. doi:10.3201/eid2207.160326

78. Lanciotti RS, Calisher CH, Gubler DJ, Chang GJ, Vorndam A V. Rapid detection and typing of dengue viruses from clinical samples by using reverse transcriptase-polymerase chain reaction. J Clin Microbiol. 1992;30: 545–51. Available: http://www.ncbi.nlm.nih.gov/pubmed/1372617

79. Grossi-Soyster EN, Cook EAJ, de Glanville WA, Thomas LF, Krystosik AR, Lee J, et al. Serological and spatial analysis of alphavirus and flavivirus prevalence and risk factors in a rural community in western Kenya. Bingham A, editor. PLoS Negl Trop Dis. 2017;11: e0005998. doi:10.1371/journal.pntd.0005998

80. Palamara GM, Childs DZ, Clements CF, Petchey OL, Plebani M, Smith MJ. Inferring the temperature dependence of population parameters: The effects of experimental design and inference algorithm. Ecol Evol. 2014;4: 4736–4750. doi:10.1002/ece3.1309

81. Team RC. R: A Language and Environment for Statistical Computing. R Found Stat Comput. 2018; Available: https://www.r-project.org